

Stochastic Video Long-term Interpolation

Qiangeng Xu

qiangenx@usc.edu

University of Southern California

Peter N. Belhumeur

belhumeur@cs.columbia.edu.com

Columbia University

Hanwang Zhang

hanwangzhang@ntu.edu.sg

Nanyang Technological University

Ulrich Neumann

uneumann@usc.edu

University of Southern California

Abstract

Video interpolation is aiming to generate intermediate sequence between two frames. While most existing studies require the two reference frames to be consecutive, we propose a stochastic learning framework that can infer a possible intermediate sequence between a long interval. Therefore, our work expands the usability of video interpolation in applications such as video long-term temporal super-resolution, missing frames repair and motion dynamic inference. Our model includes a deterministic estimation to guarantee the spatial and temporal coherency among the generated frames and a stochastic mechanism to sample sequences from possible realities. Like the studies of stochastic video prediction, our generated sequences are both sharp and varied. In addition, most of the motions are realistic and can smoothly transition from the referred start frame to the end frame.

Introduction

Video interpolation, given two frames to generate an intermediate sequence are generally applied on tasks such as temporal super-resolution and novel view interpolation (Zitnick et al. 2004). Since most existing methods rely on estimating the short-term pixel motion pattern conditioning on the two consecutive frames, when the time interval is long, they would fall short of generating complicated motion or keeping the object shape intact. Our study instead, focus on long-term intermediate sequence inference. The task can be directly applied on frame rate enhancement for low frame rate security camera and be expanded to missing frames repair and even motion planning between two target states. The difference between the setting of ours and the classic interpolation is illustrated in Fig1. Here we assume the input has the form of temporal super resolution.

In order to infer the long-term sequence, we propose to model the motion dynamic in the same manner of the video prediction. There are two major differences that makes this task very challenging: 1. Unlike the video prediction in which one can utilize powerful RNN to sequentially encode the reference frames, the temporal layout of the input frames is not continuous. 2. Video interpolation need to keep the coherency between frames in both directions. Notably, among existing video prediction studies, two of the models

Copyright © 2019, Association for the Advancement of Artificial Intelligence (www.aaai.org). All rights reserved.

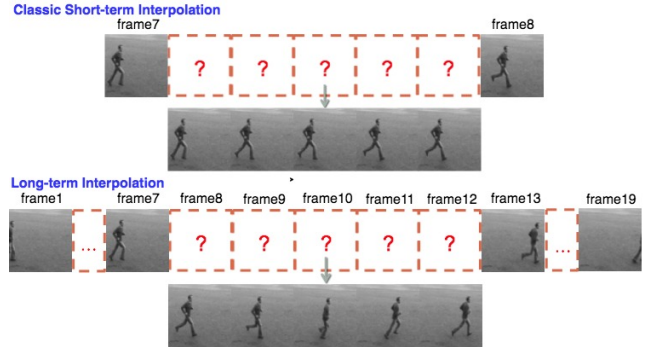


Figure 1: (a) Classic interpolation: Generates a intermediate sequence between two consecutive frames 7 and 8. (b) Long-term interpolation: Given frame 7 and 13, infer the sequence from the frame 8 to 12. A better dynamic can be obtained if incorporate extra frames. The extra frames can be 1 and 19 if the task setting is temporal super-resolution or 6 and 14 if the task setting is interval completion.

(Lu, Hirsch, and Schölkopf 2017) and (Cai et al. 2017) can also conduct long-term interpolation. However both methods, due to their forward generation mechanism, cannot address the coherency problem between the last frame and the generated sequence. To solve these challenges, we introduce a **residual bi-directional ConvLSTM** module to incorporate information from both sides. Additionally, since the sequence is conditioning not only on the two given frames, but the other ground truth frames within a range, our framework become the first one to utilize the reference frames further back to the past and further beyond the future.

Although most of the studies generate video frames in a deterministic process, the stochastic sampling process can eliminate the confusion for the network facing multiple possible futures. Instead of making a fussy prediction that compromise all possible motion patterns, a stochastic based method samples one of the solutions following a distribution. Similarly, we would generate the intermediate sequence by sampling from a **inferred distribution** in each step. The stochasticity of our task is shown in Fig2.

We propose a stochastic learning framework for long-term video interpolation. We take in two non-consecutive frames

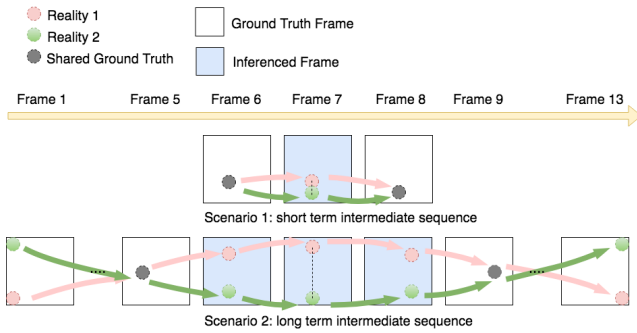


Figure 2: (A) Both scenarios have more than one possible solution. (B) The pose difference in the frame 7 between the two scenarios shows the longer intermediate sequence can have more variation. (C) In the scenario 2, if we can observe the frame 1 and 13, only one of the two paths is possible.

and more frames back to the past and further beyond and extract a dynamic pattern embedding. Then with the embedding, we use a residual bi-directional ConvLSTM network to create a reference hidden sequence that would enforce the coherency between generated sequence and ground truth frames. Conditioning on the previous generated frames and the hidden sequence, each step we infer a distribution and sample a dynamic vector from it. Combining the dynamic vector with the previous frames, we can synthesize a new frame in each step. Finally, we also apply a beneficial **movement weighted mask** in our loss function. Our contributions are summarized below:

- We are the first study generate the intermediate sequence by a stochastic process and the first study explicitly utilize the ground truth frames further beyond in the future and further back to the past for the interpolation task.
- Using a residual bi-directional ConvLSTM module to learn the information of reference frames from both sides, our framework solve the motion incoherence problem in long-term video interpolation.
- We apply a movement weighted mask in pixel loss which helps the dynamic generation against the stale content.
- We evaluate our model on various standard datasets and show that it stands out among previous frameworks and can provide sufficient variety of possible sequences.

Related Works

Video interpolation between two consecutive frames is one of the basic computer vision tasks. Although it has been thoroughly studied, it still remains a popular topic since the applications are very useful in practice and the requirement is getting higher and higher. Most of the studies such as (Ilg et al. 2017; Jiang et al. 2017) focus on generating high quality intermediate frames in a short-term interval. However, since we focus on long-term sequence inference, the existing methods cannot directly fit in due to lack of explicit motion dynamic modeling. Thus our model also refers to the ideas behind existing video prediction studies.

Video Interpolation

Short-term Video interpolation generally has three approaches: optical flow based interpolation, phase based interpolation and deep motion pixels transformation. (Herbst, Seitz, and Baker 2009; Yu et al. 2013; Ilg et al. 2017) require an accurate optical flow inference, then interpolate the content base on the inferred flow. However, under the circumstance of long time interval, optical flow estimation is known to be inaccurate. Thus estimating the motion dynamic becomes a more favorable option. The phase based methods such as (Meyer et al. 2015) modify the pixel phase to generate intermediate frames. Although the strategy of propagating phase information is elegant, the high-frequency and large content change cannot be properly handled. In the long-term setting, the inter frame change is even more drastic. Currently studies such as (Liu et al. 2017; Niklaus, Mai, and Liu 2017b; Jiang et al. 2017) use deep learning methods to infer the motion flow between the two frames. Studies of this approach can by far achieve the best result and has relatively more potential to solve our task. In our evaluation process, we use SepConv proposed in (Niklaus, Mai, and Liu 2017a) as a comparison.

Deterministic Video Prediction

The main stream video prediction methods require the input to be an short consecutive sequence and generate the deterministic future sequence by iteratively predicting next frame. (Vondrick, Pirsiavash, and Torralba 2016; Mathieu, Couprie, and LeCun 2015) use convolutional network to directly generate each pixel of the new frame, While studies such as (Srivastava, Mansimov, and Salakhudinov 2015; Finn, Goodfellow, and Levine 2016) use recurrent network to model the dynamic change in each step and improve the result drastically. (Xingjian et al. 2015) introduce a novel RNN, ConvLSTM, which has been proved to be favorable in spatial dynamic modeling. (Villegas et al. 2017; Denton and others 2017) propose to model the content and the dynamic independently, resulting in less workload for the networks and impressive result with many more time steps. (Tulyakov et al. 2017; Villegas et al. 2017) incorporate GANs(Goodfellow et al. 2014) into their model and improve the generation quality. Our model also adopt the decomposition of the motion and the content, use ConvLSTM in the motion inference and generate the frame in an iterative manner. However we don't use GANs since our study focus more on dynamic inference. We also compare our model with FSTN in (Lu, Hirsch, and Schölkopf 2017), a prediction model that can also handle interpolation task.

Stochastic Video Generation

After (Babaeizadeh et al. 2017; Henaff, Zhao, and LeCun 2017) showing the importance of the stochasticity in video prediction, later studies such as (Lee et al. 2018) also conduct the prediction in a form of stochastic sampling. The stochastic prediction process consists of a deterministic distribution inference and a dynamic vector sampling from the distribution. We also adopt this general procedure and design the loss function by maximizing a variational lower

bound. We use the modified SVG-LP introduced in (Denton and Fergus) to compare with our model, since it is one of the state-of-the-art models and very related to our study.

Methods

Formulation

Here we form our interpolation task in the setting of temporal super-resolution (shown in Fig1). A real world sequence $X_{1:N}$ is captured by a low frame rate camera. The camera can only captured frames $X_{\kappa(1+m)}$ for $\kappa = 0, 1, \dots, \lfloor N/(1+m) \rfloor$. Here m is the number of the missing frames between each 2 frames. The up-sampling rate is $\mathbf{u} = m + 1$. Our model also defines a sliding inference window with an extension factor E . Starting from frame S , a sliding window would take the ground truth frames $\mathbf{X}_{\mathbf{WR}} = \{X_{S-Eu}, X_{S-(E-1)u}, \dots, X_{S+Eu}, x_{S+(E+1)u}\}$ as input. To keep the expression uncluttered, we set $T = S + u$. Conditioning on $\mathbf{X}_{\mathbf{WR}}$, the model will sample a missing frame in each step and form a sequence $\tilde{X}_{S+1:T-1}$ in the end. The notation $\mathbf{X}_{\mathbf{WR}}$ here is the collection of all reference (ground truth) frames within a window. To our best knowledge, we are the first model considering the extended ground truth frames in the temporal super-resolution task. The rationale, as indicated in Fig2, is that we assume $P(X_{S+1:T-1}|X_{S-Eu}, \dots, X_S, X_T, \dots, X_{T+Eu})$ is a better constrained estimation than $P(X_{S+1:T-1}|X_S, X_T)$ for $P(X_{S+1:T-1}|X_{-\infty:S}, X_{T:+\infty})$. We will show the impact of those extended information in the ablation study.

The model should be able to achieve the following targets:

1. Decompose frames into content and motion features.
2. Incorporating a stochastic sampling mechanism to decide the movements.
3. The sampled frames should be coherent to each other and to the ground truth frames.
4. Although there are infinite possible realities, the model must learn from a single reality provided by the th training set and generate intermediate sequences with variability.

Training Model

Like many of the frame prediction models (Cai et al. 2017; Villegas et al. 2017; Tulyakov et al. 2017), our model decomposes each input frame into two representations by the *Encoder*. The extracted hidden vector $h_t = Enc(X_t)_{dyn}$ represent the motion associated information while the content residual $Res_t = Enc(X_t)_{ctn}$ is also saved for frame X_S and X_T . The training flow, as being described in Fig3, has 3 major sections.

The reference section, inside the purple dash line box, includes the *Extractor* and the BiLSTM, a residual bi-directional ConvLSTM. The *Extractor* takes all ground truth reference $\mathbf{X}_{\mathbf{WR}}$ and output two cell state vectors C_{start} and C_{end} . The BiLSTM would use C_{start} as the initial state of its forward cell and C_{end} of its backward cell. From S to T , each step BiLSTM would output a reference hidden vector \hat{h}_t . The whole reference hidden sequence has a conditional distribution $P(\hat{h}_{S:T}|\mathbf{X}_{\mathbf{WR}})$.

The inference section is enclosed by the crimson dash line.

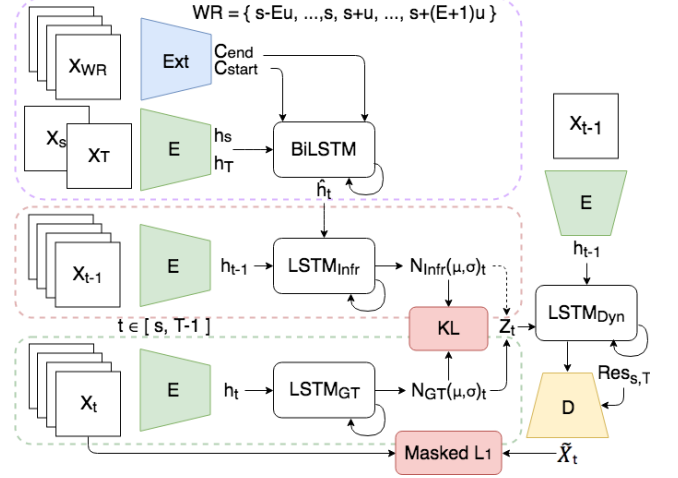


Figure 3: Training model: All green *Encoder* module share the same weight. The blue module denotes the *Extractor* and the yellow module denotes the *Decoder*. The Inference Section and the Posterior Section will produce different Z_t and therefore different frames \tilde{X}_t^{Infr} and \tilde{X}_t^{Pst} .

We extract the hidden vectors from ground truth frames $X_{S:T}$ and input the hidden vector h_{t-1} to $LSTM_{Infr}$ at time step $t - 1$. On time step t , $LSTM_{Infr}$ takes the reference vector \hat{h}_t and output a inferred distribution $P_{Infr}(z_t|X_{S:t-1}, \mathbf{X}_{\mathbf{WR}}) = N_{Infr}(\mu_t, \sigma_t)$. This section can be analogized to the prior distribution learning of (Denton and Fergus 2018) since only hidden vectors $h_{S:t-1}$ has been exposed to the RNN on step t . In their model, the distribution is $P(z_t|X_{S:t-1})$. However, our model also takes the reference vector \hat{h}_t representing the planning based on the entire $\mathbf{X}_{\mathbf{WR}}$. The distribution now becomes $P_{Infr}(z_t|X_{S:t-1}, \mathbf{X}_{\mathbf{WR}})$. To prevent the accumulation of errors, we will roll back the cell state to $t - 1$ after inferring the $N_{Infr}(\mu_t, \sigma_t)$ and input h_t extracted from ground truth X_t . This operation has been proven to be crucial to our result. On the early stage of training, a less meaningful \hat{h}_t would accumulatively disturb the cell state of $LSTM_{Infr}$, which would lead to a slow convergence.

The posterior section is outlined by the green dash line. On time t , we allow $LSTM_{GT}$ to learn a posterior distribution $P_{Pst}(z_t|X_{S:t}) = N_{GT}(\mu_t, \sigma_t)$. This section resembles the posterior training of (Babaeizadeh et al. 2017), in which the conditional distribution also shares the same form. This section enables the stochastic generation models to learn the distribution of multiple possibilities for a scenario from a single reality in the dataset. The vector h_t leaks the information of the most possible current dynamic to the $LSTM_{GT}$.

After getting $P_{Pst}(z_t|X_{S:t})$, we sample a vector z_t^{Pst} and concatenate it with h_{t-1} , then, send them into the $LSTM_{Dyn}$ to get the motion representation \tilde{X}_t . Along with content residual Res_S and Res_T , the *Decoder* will generate the \tilde{X}_t^{Pst} as $Dec(LSTM_{Dyn}(h_{S:t}), Res_S, Res_T)$. Separately, we would also sample a vector z_t^{Infr} from

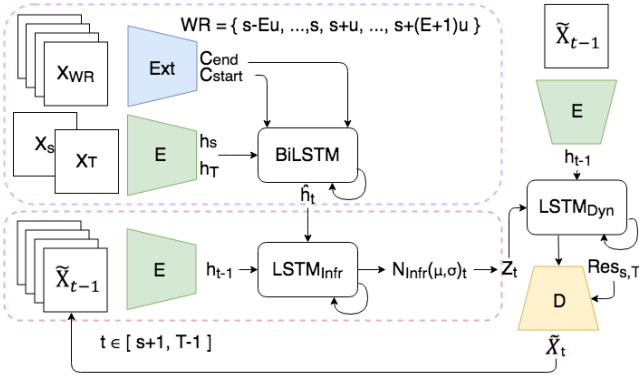


Figure 4: Generation model: only includes the Reference Section and the Inference Section. Except for first step, we use generated last frame as input to the Inference Section

$P_{Infr}(z_t|X_{S:t-1}, \mathbf{X}_{WR})$, then use a copy of $LSTM_{Dyn}$ to get a \tilde{X}_t^{Infr} in the end. The gradient won't change the weights of $LSTM_{Dyn}$ through its copy.

Generation Model

Since the missing ground truth frames are not available and we cannot obtain the X_t frame at time t , we would use the inference section to sample the z_t . The model work flow is shown in Fig4. Except for the first step, in which we have the ground truth frame X_S , the generated frame from last step would serve as the input to both $LSTM_{Infr}$ and $LSTM_{Dyn}$. The $\hat{h}_{s+1:T-1}$ produced by the reference section will help keep the coherency at the end (between \tilde{X}_{T-1}^{Infr} and X_T) by preventing the dynamic from gradually straying away against the possible trajectories.

Objectives

Since ideally the \tilde{X}_t^{Pst} should reconstruct the real X_t , we introduce a pixel loss. Studies such as (Lee et al. 2018) state although the L_2 loss generally give better result on SSIM and PSNR, it will produce blurry predictions. Here we choose to use $L_1(X_t, \tilde{X}_t^{Pst})$. In the testing phase, we can only use the inference section, thus we need the $P_{Infr}(z_t|X_{S:t-1}, \mathbf{X}_{WR})$ to be similar enough to the $P_{Pst}(z_t|X_{S:t})$. Therefore here we also add two KL divergences between these two distributions. Besides, after P_{Infr} getting stable, we observe that directly imposing a pixel loss on \tilde{X}_t^{Infr} can further improve the quality. Our final Objective is to minimize the following combined loss:

$$L_C = \sum_{t=s+1}^{T-1} [\beta \cdot L_1(X_t, \tilde{X}_t^{Pst}) + (1 - \beta) \cdot L_1(X_t, \tilde{X}_t^{Infr}) + \alpha \cdot D_{KL}(P_{Pst}||P_{Infr}) + \gamma \cdot D_{KL}(P_{Infr}||P_{Pst})] \quad (1)$$

The β balances the posterior reconstruction and the inference reconstruction, while the α and the γ determines the trade-off between the reconstruction and the distributions' similarity. Both the forward and the reverse KL-divergence of P_{Infr} and P_{Pst} achieve the minimum when the two distributions are equal. However, according to (Fox and Roberts

2012), since $D_{KL}(P_{Pst}||P_{Infr})$ is sampled on P_{Pst} , it will penalize more when P_{Pst} is large and P_{Infr} is small, thus leads to a P_{Infr} with richer diversity. On the other hand, $D_{KL}(P_{Infr}||P_{Pst})$ will make the inference more accurate when P_{Infr} has large value. To better serve our task, we decide to keep both terms to strike a balance between accuracy and diversity. To theoretically validate this loss function, We use the variational lower bound which is similar to the VAE (Kingma and Welling 2013). To maximize a sequence's probability with the form $\log P(\tilde{X}_{S:T})$. We can maximize its variational lower bound (See Appendix A for the proof of the lower bound):

$$\sum_{t=s}^{T-1} \mathbb{E}_{Q(z_t)} \log P(\tilde{X}_t | \tilde{X}_{S:t-1}, z_{S:t}) - \int_z Q(z_{S:T}) \log \frac{Q(z_{S:T})}{P(z_{S:T})} \quad (2)$$

Since we are interested in maximizing $\log P(\tilde{X}_{S:T-1}^{Infr})$, we can fit P_{Pst} and P_{Infr} into (2)'s $P(z_{S:t})$ and $Q(z_{S:T})$:

$$\log P(\tilde{X}_{S:T-1}^{Infr}) \geq \sum_{t=s}^{T-1} \left[\mathbb{E}_{P_{Infr}(z_t)} \log P(X_t^{Infr} | X_{S:t-1}^{Infr}, z_{S:t}^{Infr}) - D_{KL}(P_{Infr}(z_t | X_{S:t-1}^{Infr}, \mathbf{X}_{WR}) || P_{Pst}(z_t | X_{S:t}^{Pst})) \right] \quad (3)$$

However, if we only maximize the lower bound above, the $LSTM_{GT}$ will tend to ignore the information in X_t since it has not been exposed to $LSTM_{Infr}$. The $P_{Infr}(z_t)$ and $P_{Infr}(z_t)$ will degenerate to a convenient fixed value to lower the D_{KL} . Thus we also need to improve the reconstruction of X_t and maximize $\log P(\tilde{X}_{S:T-1}^{Pst})$. Similarly, we fit P_{Infr} and Q_{Pst} into (2)'s $P(z_{S:t})$ and $Q(z_{S:T})$ to get its variational lower bound :

$$\log P(\tilde{X}_{S:T-1}^{Pst}) \geq \sum_{t=s}^{T-1} \left[\mathbb{E}_{Q_{Pst}(z_t)} \log P(X_t^{Pst} | X_{S:t-1}^{Pst}, z_{S:t}^{Pst}) - D_{KL}(Q_{Pst}(z_t | X_{S:t-1}^{Pst}) || P_{Infr}(z_t | X_{S:t-1}^{Infr}, \mathbf{X}_{WR})) \right] \quad (4)$$

We can see in the loss function (1): the first term is to help increase the first term of (4). The second loss term is aiming to improve the first term of (3). The third and the fourth loss term would penalize the second terms in (4) and (3). More details of the explanation and deduction can be found in Appendix B.

Residual Bi-directional ConvLSTM

(Xingjian et al. 2015) has shown Convolutional LSTM a very powerful structure for spatial sequence inference. Besides, (Bahdanau, Cho, and Bengio 2014) has shown the bi-directional structure a powerful structure to bring the future information back to current step. Our reference section is essentially doing a sequence completion. Here we need to transfer an incomplete sequence $h_S, \mathbf{0}, \dots, \mathbf{0}, h_T$ to a completed sequence $\hat{h}_{S:T}$ with extra help from \mathbf{X}_{WR} . Stacking multiple layers of RNN has been proven to be powerful in sequence inference. However in our case, features on the bottom layer $h_S, \mathbf{0}, \dots, \mathbf{0}, h_T$ share a same feature space with $\hat{h}_{S:T}$ on the top layer. Thus, inspired by (He et al. 2015), we decide to add an residual connection between each layers to bring the bottom feature directly to the top. In the end, BiLSTM combines all the three structures, the ConvLSTM, the bi-directional RNN and the residual connections.

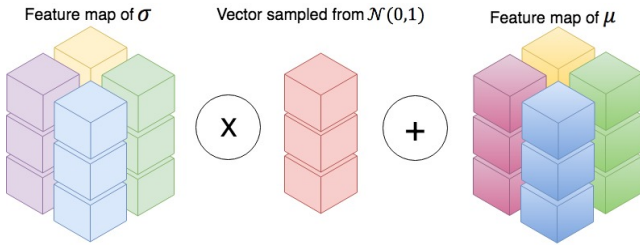


Figure 5: The sampled vector will be applied on all location.

Sampling the Dynamic

In order to train Q_t^{Pst} and P_t^{Infr} , we use the reparameterization trick from (Kingma and Welling 2013) and set them as Gaussian distributions $N_{Infr}(\mu_t, \sigma_t)$ and $N_{GT}(\mu_t, \sigma_t)$. A Gaussian distribution can be mapped to any distribution through a function with sufficient complication. After inferred the μ_t and σ_t , we will sample a vector from a normal distribution and calculate the Gaussian. The mechanism is based on the previous stochastic frame prediction studies such as (Denton and Fergus 2018). However, we consider a spatial vector as a stronger representation of movement. Different locations in one frame may have different stochasticity and pattern, uniformly draw a sample following the same distribution everywhere will hinder the modeling. Thus, we introduce a spacial vector sampling process (shown in Fig5). Instead of using 2D vectors, we use spacial feature maps for μ_t and σ_t . We multiple the sampled vector on each location of σ_t , then add on the μ_t to get the Z_t .

Experiments

We test our model on three datasets representing different dynamics: Stochastic Moving MNIST(SM-MNIST) for rigid body object with random momentum, KTH Action Database for deformable object (human body) and BAIR robot pushing dataset for abrupt stochastic movement. We conduct quantitative evaluation not only using the classic quality metrics such as structural similarity (SSIM) and Peak Signal-to-Noise Ratio (PSNR), but also a new metric LMS. A generated sequence different from the ground truth (low SSIM and PSNR) can still be valid if the dynamic pattern make sense. Thus we introduce the last momentum similarity (LMS) which is the MSE between the optic flow of X_{T-1} and X_T and the optical flow of \tilde{X}_{T-1}^{Infr} and X_T . We find LMS is a good indicator of the video coherency since no matter how the dynamic being sampled, the object should go back to its track and make a smooth transition to X_T . We also qualitatively compare our samples with other state-of-the-art models such as SepConv(Niklaus, Mai, and Liu 2017a) a high performance interpolation model, FSTN(Lu, Hirsch, and Schölkopf 2017) a deterministic frame generation model with capability of interpolation and SVP(Denton and Fergus 2018) representing stochastic video generation model applied to interpolation. Since FSTN and SVP are not originally aiming to solve our task, we also provide last frame’s representation for them in each time step. In addition, We also conduct ablation studies by taking off the spa-

cial sampling and not using X_{WR} . More video results have been included in the supplementary material.

Model Architecture and training details

The *Encoder*, the *Extractor* and the *Decoder* uses the same architecture of DCGAN (Radford, Metz, and Chintala 2015). For step S and T , all layer’s feature map of the *Encoder* will be gathered as a multi-scale residuals Res_S and Res_T to help reconstruct the static content. $LSTM_{Infr}$, $LSTM_{Pst}$ and $LSTM_{Dgn}$ use the structure of one layer ConvLSTM. Other structure and training details can be found in Appendix C.

In addition, we apply a **movement weighted mask** on each location of the pixel loss. If a pixel value stay the same, the weight is 1 on that location. However if the location has pixel value change, we either set the weight to 0 if it’s a flickering pixel (determined by its isolation level) or to $\eta > 1$ to emphasize more on the moving region. Through this operation, we:(1) denoise the dynamic information, (2) encourage the dynamic learning to prevent the static sequence generation. We also plot the mask in results such as Fig10.

Stochastic Moving MNIST (SM-MNIST)

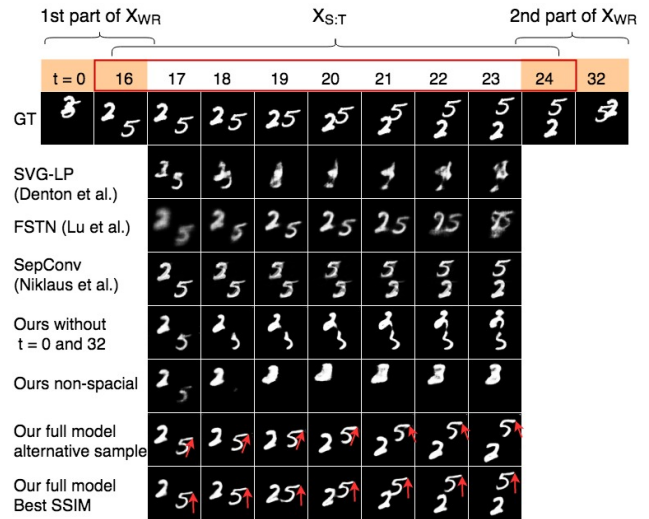


Figure 6: Only our full model and non-spacial are capable to utilize frame 0 and 32. The sampled sequence with best SSIM is picked and shown in the last row. The digit 5 in the best sequence follows the same upward trajectory as ground truth. In another sampled sequence shown as the second last row, the digit 5 goes upper right and then bounce upper left.

Different from the moving MNIST, the SM-MNIST introduced by (Denton and Fergus 2018) is generated by randomly picking two digits, setting their initial position and speed. After bouncing off the wall, the digit will randomly pick a new speed and direction. Since the dataset contains no pixel noise and no static content, applying the weighted mask is unnecessary. Although the dataset only contains non-deformable objects moving in a simple pattern, it turns out to be very challenging for all methods. The Avg PSNR,

	SM-MNIST			BAIR			KTH		
	Avg PSNR	Avg SSIM	Avg LMS	Avg PSNR	Avg SSIM	Avg LMS	Avg PSNR	Avg SSIM	Avg LMS
Our full model	21.025	0.926	0.303	21.432	0.880	1.05	29.190	0.901	0.248
Ours without 0 & 32	19.857	0.906	0.353	19.694	0.852	1.36	26.907	0.831	0.478
Ours non-spatial	13.207	0.752	6.394	19.938	0.865	1.159	29.366	0.896	0.276
SVG-LP	13.543	0.741	5.393	18.648	0.846	1.891	28.131	0.883	0.539
FSTN	14.730	0.765	3.773	19.908	0.850	1.332	29.431	0.899	0.264
SepConv	14.759	0.775	2.160	21.615	0.877	1.237	29.210	0.904	0.261

Table 1: Result of metrics averaging over all frames. Here we report the metrics score of the best sample for our model.

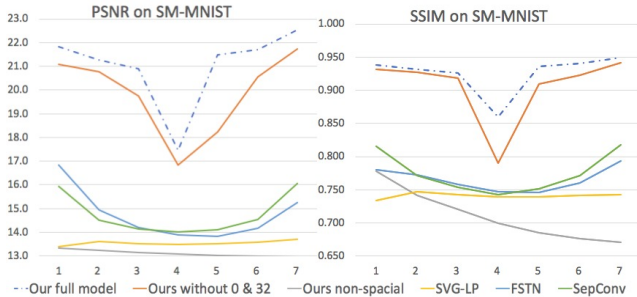


Figure 7: Metrics averaging overall all SM-MNIST's test sequences for each step.

SSIM and LMS over all frames are shown in Table 1. We also plot the average metrics for each step in Fig 7 and pick a example Fig 6 to qualitatively evaluate our methods. For the situation when two frames 16 and 24 having drastic position difference, interpolation models such as SepConv would suffer from moving the pixel based on the proximity between the two frames. We can see the digit 2 and 5 gradually transfer to each other since 2 in the frame 16 is closer to digit 5 in the frame 24. The deterministic generation model FSTN cannot handle the sequence with such uncertainty (random speed and direction bouncing off the wall), thus the network get confused and generate blurry result. The SVG-LP also cannot converge in this setting even giving the final frame 24 in each step. It doesn't have a proper planning module like our BiLSTM to lead the sequence to the final frame. Since SM-MNIST has multiple moving components, non spatial representation cannot support different dynamics in different area and lead to poor result. The example of "Ours non-spatial" in Fig 6 even shows the two digits collapsing into one component then move toward the final frame due to lack of spatial sampling capability. Finally, our full model can learn the bouncing rule and provide reasonable alternative realities. Although our randomly sampled sequence diverges from the ground truth, this sequence can still keep the coherency between the frame 16 and 24, moving under a reasonable pattern.

BAIR robot pushing dataset

The BAIR robotic pushing dataset (Ebert et al. 2017) contains sequences of a robot arm pushing various objects in the RGB domain. The movements of the arm don't follow smooth trajectories and the directions change are prompt. In Table 1 although our model marginally outperform other

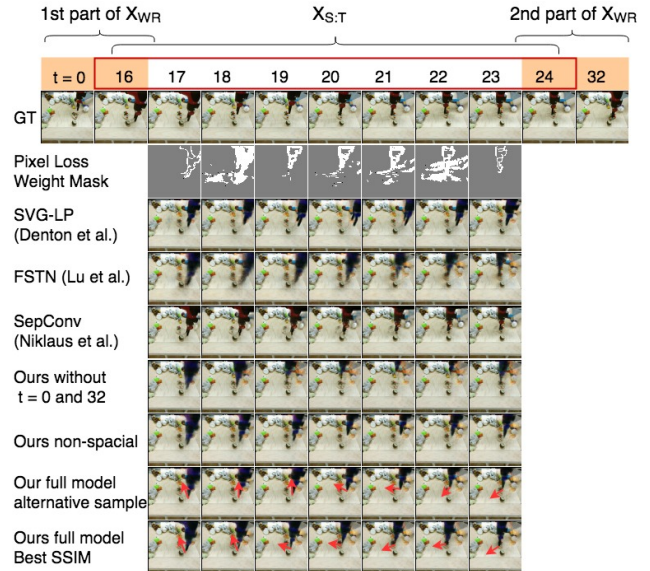


Figure 8: The arm in the best sequence follows the same upward left then downward left movement as the ground truth has. In another sampled sequence, the arm goes straight up and then straight left, finally goes downward left.

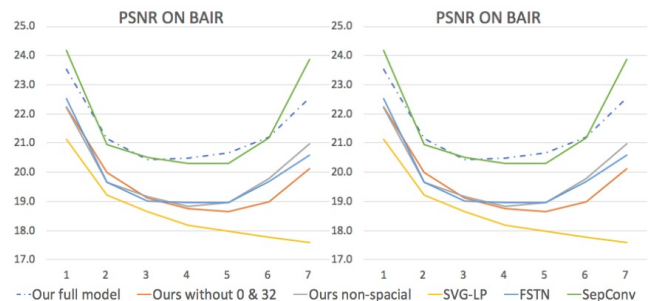


Figure 9: Metrics averaging overall all BAIR's test sequences for each step.

models on SSIM, we can see SepConv achieves the best PSNR. Shown in Fig 8, since the SepConv relies more on pixel proximity, the shape of static objects in this method preserved the best. However, the result of SepConv in Fig 8 loses the stochasticity while its movement is simplified to a straight sliding. The frames in the middle suffer the most in all metrics (Fig.9) due to this sliding inclination. The

stochasticity of the arm’s movement make it hard for SVG-LP’s arm to go back to the final frame and for FSTN to generate sharp shape in a deterministic manner. Our model without spatial sampling creates less sharp object since all area will be affected by the inferred dynamic. On the other hand, the result of our model without referring frame 0 and 32 would diverge too much away from the ground truth movement. Our full model can not only sample a similar sequence but a reasonable alternative movement shown in Fig8.

KTH Action Dataset

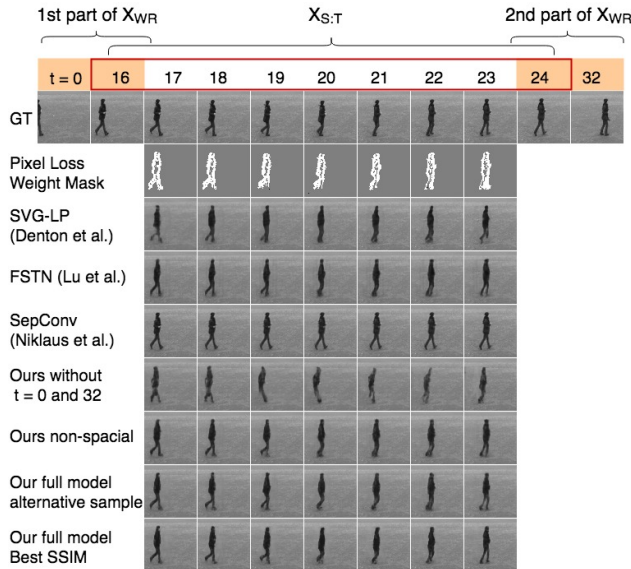


Figure 10: SepConv although generates sharp frames, its sliding tendency will cause dynamic errors and higher LMS.

The KTH Action dataset (Schuldt, Laptev, and Caputo 2004) is a standard video generation dataset containing real-world videos of six human actions. Although the background is uniform, there are still some pixel noise. The moving parts in a frame includes only a small amount of pixel which can lead to stale frame generation. We find setting the mask’s weight η to 5 on moving pixel and 0 on noise is very beneficial. Since most movements follow repetitive patterns (run in a stable pace, etc.) We can see the FSTN achieves the best PSNR and SepConv achieves the best SSIM in Table.1. However, if the frame 16 and 24 having a similar pose, SepConv will freeze the pose and slide the object to its new position (Shown in Fig10). Indicated by the example in Fig11), the result of deterministic method FSTN contains blurry pixels on moving region although it keep the static part sharp. Our model without referring to the frame 0 and 32 suffers from uncertainty shown in Fig10. Our full model is able to sample a sequence move under a similar pattern as the ground truth. Even a sample shown in the second last row in Fig11 can have different dynamics in the middle, the initial and the final movement would stick to the ground truth thus result in a outstanding LMS over other methods.

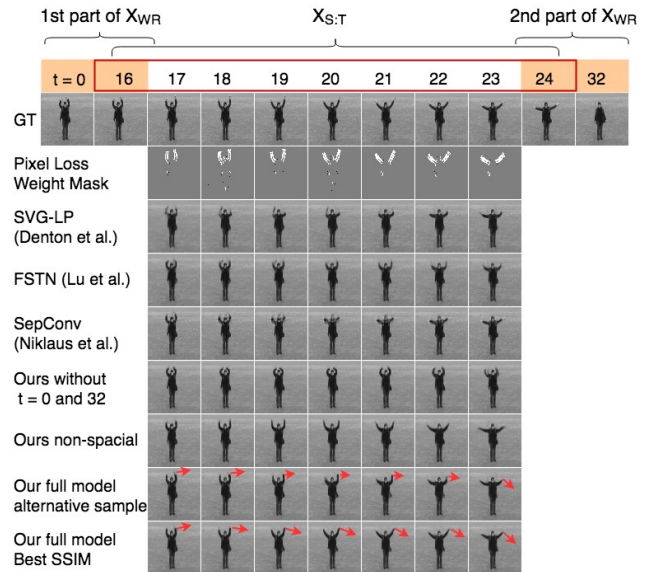


Figure 11: Our best sample keep the arm straight. In another sequence, the forearm bend first then straight in the end.

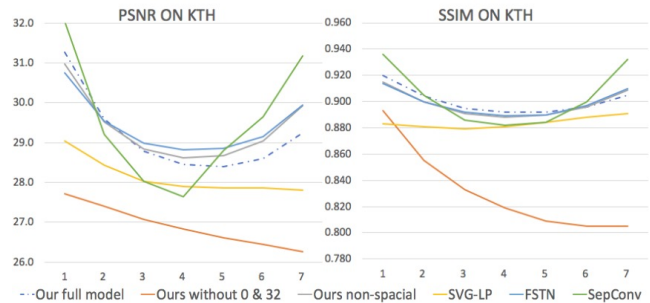


Figure 12: Metrics averaging overall all KTH’s sequences for each step. The SepConv’s performance drop drastically in the middle frames while our model can keep stable.

Conclusions and Future Work

We propose an stochastic learning framework that can infer long-term intermediate sequence between frames. The framework contains three major sections. The reference section enable us to become the first study utilizing extra reference frames beyond the start and the final frames. Based on stochastic generation models, The inference and the posterior sections are driven by our novel objective function and enable our model to sample reasonable sequences that preserve the contingency and the variety. Ablation study and comparisons with other models have been conducted on three datasets. In the quantitative evaluation, the best samples of our model achieve good performance. We also propose a new metric LMS for the sequence coherency. The qualitative evaluation shows our model can provide reasonable alternative realities in a long-term interval. Currently, same as other video generation models, our framework cannot achieve good performance on high quality videos. On the other hand, the classic interpolation models still dom-

inate the high quality short-term interpolation. The future work on improving the video quality in long-term interpolation would be very meaningful.

References

- [Babaeizadeh et al. 2017] Babaeizadeh, M.; Finn, C.; Erhan, D.; Campbell, R. H.; and Levine, S. 2017. Stochastic variational video prediction. *arXiv preprint arXiv:1710.11252*.
- [Bahdanau, Cho, and Bengio 2014] Bahdanau, D.; Cho, K.; and Bengio, Y. 2014. Neural machine translation by jointly learning to align and translate. *arXiv preprint arXiv:1409.0473*.
- [Cai et al. 2017] Cai, H.; Bai, C.; Tai, Y.-W.; and Tang, C.-K. 2017. Deep video generation, prediction and completion of human action sequences. *arXiv preprint arXiv:1711.08682*.
- [Denton and Fergus 2018] Denton, E., and Fergus, R. 2018. Stochastic video generation with a learned prior. *arXiv preprint arXiv:1802.07687*.
- [Denton and others 2017] Denton, E. L., et al. 2017. Unsupervised learning of disentangled representations from video. In *Advances in Neural Information Processing Systems*, 4414–4423.
- [Ebert et al. 2017] Ebert, F.; Finn, C.; Lee, A. X.; and Levine, S. 2017. Self-supervised visual planning with temporal skip connections. *arXiv preprint arXiv:1710.05268*.
- [Finn, Goodfellow, and Levine 2016] Finn, C.; Goodfellow, I.; and Levine, S. 2016. Unsupervised learning for physical interaction through video prediction. In *Advances in neural information processing systems*, 64–72.
- [Fox and Roberts 2012] Fox, C. W., and Roberts, S. J. 2012. A tutorial on variational bayesian inference. *Artificial intelligence review* 38(2):85–95.
- [Goodfellow et al. 2014] Goodfellow, I.; Pouget-Abadie, J.; Mirza, M.; Xu, B.; Warde-Farley, D.; Ozair, S.; Courville, A.; and Bengio, Y. 2014. Generative adversarial nets. In *Advances in neural information processing systems*, 2672–2680.
- [He et al. 2015] He, K.; Zhang, X.; Ren, S.; and Sun, J. 2015. Deep residual learning for image recognition. *corr*, vol. abs/1512.03385.
- [Henaff, Zhao, and LeCun 2017] Henaff, M.; Zhao, J.; and LeCun, Y. 2017. Prediction under uncertainty with error-encoding networks. *arXiv preprint arXiv:1711.04994*.
- [Herbst, Seitz, and Baker 2009] Herbst, E.; Seitz, S.; and Baker, S. 2009. Occlusion reasoning for temporal interpolation using optical flow. *Department of Computer Science and Engineering, University of Washington, Tech. Rep. UW-CSE-09-08-01*.
- [Ilg et al. 2017] Ilg, E.; Mayer, N.; Saikia, T.; Keuper, M.; Dosovitskiy, A.; and Brox, T. 2017. FlowNet 2.0: Evolution of optical flow estimation with deep networks. In *IEEE conference on computer vision and pattern recognition (CVPR)*, volume 2, 6.
- [Jiang et al. 2017] Jiang, H.; Sun, D.; Jampani, V.; Yang, M.-H.; Learned-Miller, E.; and Kautz, J. 2017. Super slo-mo: High quality estimation of multiple intermediate frames for video interpolation. *arXiv preprint arXiv:1712.00080*.
- [Kingma and Welling 2013] Kingma, D. P., and Welling, M. 2013. Auto-encoding variational bayes. *arXiv preprint arXiv:1312.6114*.
- [Lee et al. 2018] Lee, A. X.; Zhang, R.; Ebert, F.; Abbeel, P.; Finn, C.; and Levine, S. 2018. Stochastic adversarial video prediction. *arXiv preprint arXiv:1804.01523*.
- [Liu et al. 2017] Liu, Z.; Yeh, R. A.; Tang, X.; Liu, Y.; and Agarwala, A. 2017. Video frame synthesis using deep voxel flow. In *ICCV*, 4473–4481.
- [Lu, Hirsch, and Schölkopf 2017] Lu, C.; Hirsch, M.; and Schölkopf, B. 2017. Flexible spatio-temporal networks for video prediction. In *Proceedings of the IEEE Conference on Computer Vision and Pattern Recognition*, 6523–6531.
- [Mathieu, Couprie, and LeCun 2015] Mathieu, M.; Couprie, C.; and LeCun, Y. 2015. Deep multi-scale video prediction beyond mean square error. *arXiv preprint arXiv:1511.05440*.
- [Meyer et al. 2015] Meyer, S.; Wang, O.; Zimmer, H.; Grosse, M.; and Sorkine-Hornung, A. 2015. Phase-based frame interpolation for video. In *Proceedings of the IEEE Conference on Computer Vision and Pattern Recognition*, 1410–1418.
- [Niklaus, Mai, and Liu 2017a] Niklaus, S.; Mai, L.; and Liu, F. 2017a. Video frame interpolation via adaptive convolution. In *IEEE Conference on Computer Vision and Pattern Recognition*, volume 1, 3.
- [Niklaus, Mai, and Liu 2017b] Niklaus, S.; Mai, L.; and Liu, F. 2017b. Video frame interpolation via adaptive separable convolution. *CoRR* abs/1708.01692.
- [Radford, Metz, and Chintala 2015] Radford, A.; Metz, L.; and Chintala, S. 2015. Unsupervised representation learning with deep convolutional generative adversarial networks. *arXiv preprint arXiv:1511.06434*.
- [Schuldt, Laptev, and Caputo 2004] Schuldt, C.; Laptev, I.; and Caputo, B. 2004. Recognizing human actions: a local svm approach. In *Pattern Recognition, 2004. ICPR 2004. Proceedings of the 17th International Conference on*, volume 3, 32–36. IEEE.
- [Srivastava, Mansimov, and Salakhudinov 2015] Srivastava, N.; Mansimov, E.; and Salakhudinov, R. 2015. Unsupervised learning of video representations using lstms. In *International conference on machine learning*, 843–852.
- [Tulyakov et al. 2017] Tulyakov, S.; Liu, M.-Y.; Yang, X.; and Kautz, J. 2017. Mocogan: Decomposing motion and content for video generation. *arXiv preprint arXiv:1707.04993*.
- [Villegas et al. 2017] Villegas, R.; Yang, J.; Hong, S.; Lin, X.; and Lee, H. 2017. Decomposing motion and content for natural video sequence prediction. *arXiv preprint arXiv:1706.08033*.
- [Vondrick, Pirsaviash, and Torralba 2016] Vondrick, C.; Pirsaviash, H.; and Torralba, A. 2016. Generating videos with scene dynamics. In *Advances In Neural Information Processing Systems*, 613–621.

[Xingjian et al. 2015] Xingjian, S.; Chen, Z.; Wang, H.; Yeung, D.-Y.; Wong, W.-K.; and Woo, W.-c. 2015. Convolutional lstm network: A machine learning approach for precipitation nowcasting. In *Advances in neural information processing systems*, 802–810.

[Yu et al. 2013] Yu, Z.; Li, H.; Wang, Z.; Hu, Z.; and Chen, C. W. 2013. Multi-level video frame interpolation: Exploiting the interaction among different levels. *IEEE Transactions on Circuits and Systems for Video Technology* 23(7):1235–1248.

[Zitnick et al. 2004] Zitnick, C. L.; Kang, S. B.; Uyttendaele, M.; Winder, S.; and Szeliski, R. 2004. High-quality video view interpolation using a layered representation. In *ACM transactions on graphics (TOG)*, volume 23, 600–608. ACM.

Appendices

Appendix A. Proof of variational lower bound

$P(\tilde{X}_{s:T})$ can be deemed as the probability of any sequence data. The logarithm of this probability has the following variational lower bound:

$$\log P(\tilde{X}_{s+1:T-1}) = \log \int_z P(\tilde{X}_{s+1:T-1} | z_{s:T-1}) P(z_{s:T-1}) \frac{Q(z_{s:T})}{Q(z_{s:T})} \quad (5)$$

$$= \log \mathbb{E}_{Q(z_{s:T})} \frac{P(\tilde{X}_{s+1:T-1} | z_{s:T-1}) P(z_{s:T})}{Q(z_{s:T})} \quad (6)$$

$$\geq \mathbb{E}_{Q(z_{s:T})} \frac{P(\tilde{X}_{s+1:T-1} | z_{s:T-1}) P(z_{s:T})}{Q(z_{s:T})} \quad (7)$$

$$= \mathbb{E}_{Q(z_{s:T})} \log P(\tilde{X}_{s+1:T-1} | z_{s:T-1}) - E_{Q(z_{s:T})} \frac{Q(z_{s:T})}{P(z_{s:T})} \quad (8)$$

$$= \mathbb{E}_{Q(z_{s:T})} \log \prod_t P(\tilde{X}_t | \tilde{X}_{s:t-1}, z_{s:t}) - \int_z Q(z_{s:T}) \log \frac{Q(z_{s:T})}{P(z_{s:T})} \quad (9)$$

$$= \sum_{t=s}^{T-1} \mathbb{E}_{Q(z_t)} \log P(\tilde{X}_t | \tilde{X}_{s:t-1}, z_{s:t}) - \int_z Q(z_{s:T}) \log \frac{Q(z_{s:T})}{P(z_{s:T})} \quad (10)$$

Appendix B. Explanation of the deduction and the reasoning

In our model, since the output from the Inference section is the output in generation phase. We are most interested in maximizing $\log P(\tilde{X}_{s:T-1}^{Infr})$. Since the lower bound shown in Appendix A will hold for any form of the distribution, we can fit P_{Pst} and P_{Infr} into (10)’s $P(z_{s:T})$ and $Q(z_{s:T})$:

$$\log P(\tilde{X}_{s:T-1}^{Infr}) \geq \sum_{t=s}^{T-1} \left[\mathbb{E}_{P_{Infr}(z_t)} \log P(X_t^{Infr} | X_{s:t-1}^{Infr}, z_{s:t}^{Infr}) \right.$$

$$\left. - \int_{z_{s:T-1}^{Infr}} P_{Infr} \cdot \log \frac{P_{Infr}}{P_{Pst}} \right] \quad (11)$$

The integration part (KL divergence of the sequence) in the above inequality can be decomposed as:

$$\begin{aligned} & \int_{z_{s:T-1}^{Infr}} P_{Infr} \cdot \log \frac{P_{Infr}}{P_{Pst}} \\ &= \int_{z_s^{Infr}} \int_{z_{s+1}^{Infr}} \cdots \int_{z_{T-1}^{Infr}} \left[\prod_{t=s}^T P_{Infr}(z_t | X_{s:t-1}^{Infr}, X_{WR}) \right. \\ & \quad \left. \cdot \sum_t \log \frac{P_{Infr}(z_t | X_{s:t-1}^{Infr}, X_{WR})}{P_{Pst}(z_t | X_{s:t}^{Pst})} \right] \end{aligned} \quad (12)$$

$$= \sum_{t=1}^{T-1} \mathbb{E}_{P_{Infr}(z_t | X_{s:t-1}^{Infr}, X_{WR})} \log \frac{P_{Infr}(z_t | X_{s:t-1}^{Infr}, X_{WR})}{P_{Pst}(z_t | X_{s:t}^{Pst})} \quad (13)$$

$$= \sum_{t=1}^{T-1} D_{KL}(P_{Infr}(z_t | X_{s:t-1}^{Infr}, X_{WR}) || P_{Pst}(z_t | X_{s:t}^{Pst})) \quad (14)$$

Therefore if we put (14) back to the lower bound (11), the logarithm of the probability we want to maximize becomes:

$$\begin{aligned} \log P(\tilde{X}_{s:T-1}^{Infr}) &= \sum_{t=s}^{T-1} \left[\mathbb{E}_{P_{Infr}(z_t)} \log P(X_t^{Infr} | X_{s:t-1}^{Infr}, z_{s:t}^{Infr}) \right. \\ & \quad \left. - D_{KL}(P_{Infr}(z_t | X_{s:t-1}^{Infr}, X_{WR}) || P_{Pst}(z_t | X_{s:t}^{Pst})) \right] \end{aligned} \quad (15)$$

Since sometimes neural network has the tendency to use the easiest way to fit the objective, if we only maximize (15), the $LSTM_{GT}$ will ignore the information brought by X_t . The $P_{Infr}(z_t)$ and $P_{Infr}(z_t)$ will degenerate to a convenient fixed value to lower the D_{KL} . Our Inference and Posterior Section then will be resemble the SVG-FP, which is a simpler version of SVG-LP using fixed prior distribution.

To prevent the degeneration, we also need to maximize the probability of the reconstructed frame \tilde{X}_t^{Pst} to force the newly observed dynamic from X_t being carried in P_{Pst} . Here we fit P_{Infr} and Q_{Pst} into (10)’s $P(z_{s:t})$ and $Q(z_{s:T})$ and we end up also maximizing:

$$\begin{aligned} \log P(\tilde{X}_{s:T-1}^{Pst}) &= \sum_{t=s}^{T-1} \left[\mathbb{E}_{P_{Pst}(z_t)} \log P(X_t^{Pst} | X_{s:t-1}^{Pst}, z_{s:t}^{Pst}) \right. \\ & \quad \left. - D_{KL}(P_{Pst}(z_t | X_{s:t-1}^{Pst}) || P_{Infr}(z_t | X_{s:t-1}^{Infr}, X_{WR})) \right] \end{aligned} \quad (16)$$

The deduction process of this result is the same as the transformation from (11) to (15). Thus we design a objective function to maximize both of (15) and (16) at the same time.

Appendix C. Feature dimensions and training details

The output dimensions of our modules are listed in Table3. All datasets have been trained with frame dimensions of

64×64 . We use standard Adam optimizer with 0.5 as the first momentum decay rate. All the hyper parameter settings for different datasets are shown in 2. The β is initially set to 1 and gradually reduce to 0.4.

Training Parameters	SMMNIST	BAIR	KTH
α	0.002	0.0002	0.0002
γ	0.001	0.0001	0.0001
β	1 to 0.4	1 to 0.4	1 to 0.4
Mask Weight η	N/A	2	5

Table 2: Hyper parameters for training on different datasets

Feature	Dimension 1	Dimension2	Dimension3
C_{start}	4	4	256
C_{end}	4	4	256
h_t	4	4	256
\hat{h}_t	4	4	256
σ_t SMMNIST & KTH	4	4	32
μ_t SMMNIST & KTH	4	4	32
σ_t BAIR	4	4	64
μ_t BAIR	4	4	64

Table 3: Dimensionality of different features